J. Phys.: Condens. Matter 4 (1992) 4959–4970. Printed in the UK

Electron intersubband scattering by confined and localized phonons in real quantum wires

R Mickevičius†, V V Mitin†, K W Kim‡, Michael A Stroscio§ and Gerald J Iafrate§

† Department of Electrical and Computer Engineering, Wayne State University, Detroit, MI 48202, USA

‡ Department of Electrical and Computer Engineering, North Carolina State University, Raleigh, NC 27695, USA

§ U.S. Army Research Office, PO Box 12211, Research Triangle Park, NC 27709, USA

Received 16 December 1991

Abstract. The present study deals with electron intersubband scattering in real quantum wire structures. Both the multi-subband structure and confined phonon modes are considered together. The rates of scattering by confined longitudinal-optical (LO) phonons and by surface-optical (SO) phonons are calculated taking into account all possible LO phonon modes as well as all possible electron intersubband transitions. The estimations of transition rates for GaAs/AlAs QWIS have shown that intrasubband electron scattering and most intersubband transitions are due primarily to scattering by confined LO phonons, but in resonant intersubband transitions the contribution of SO phonons may be dominant when the phonon energy is close to the intersubband energy separation. Moreover, electron–SO-phonon scattering might play an important part in low-temperature electron transport because the GaAs-like SO mode is shifted towards lower frequencies compared with that of LO phonons. The energy dependence of the total scattering rate in an ideal quantum wire exhibits multiple sharp peaks related to each intersubband transition. These peaks originate from the resonant nature of the density of states in ideal one-dimensional systems. It is demonstrated that in real quantum wires with variable thickness the resonant peaks broaden or even disappear due to variation of subband energies.

1. Introduction

The progress in semiconductor technology has provided the means to fabricate the so-called quantum wires (QWIS) with quasi-one-dimensional (1D) structures. It has been suggested that QWIS will exhibit carrier mobilities well above 10^6 cm^2 V^{-1} s^{-1} [1], but these high values of the mobility have not yet been observed experimentally. The expected enhancement of the carrier mobility in QWIS should stem from the restriction of momentum space to one dimension as well as the resulting reduction of final states for scattered electrons. This point, however, needs to be clarified. Despite the rapidly growing number of publications on QWIS, the theoretical investigations of electron transport controlled by optical phonon scattering are limited either to the case of the extreme quantum limit (EQL) wherein only one subband is considered [2–4] and/or to the case of scattering by bulk three-dimensional (3D) phonon modes [5–7]. However, due to technological limitations the confinement of electrons is relatively weak and electrons can populate upper subbands at higher temperatures or in the hot-electron

0953-8984/92/214959+12$04.50

regime. On the other hand, recent experiments evidently demonstrate the presence of surface-optical (SO) modes [8] and phonon confinement [9]. The other significant flaw in theoretical studies of QWIS is that they deal with ideal 1D systems with fixed subband energies. A unique feature of ideal QWIS is the well-pronounced resonant nature of electron scattering as a result of multiple sharp peaks (diverging to infinity) on energy dependence of the total electron scattering rate. These peaks originate from the resonant behaviour of the density of states in ideal QWI structures and each peak is related to a particular intrasubband or intersubband transition to the bottom of the corresponding subband. Real QWIS, however, always have variable thickness along the structure. Generally, electron beam or x-ray lithography on a quantum well surface, with subsequent reactive ion (beam) etching, is used for QWI frabrication [10, 11]. State-of-the-art technology allows the quantum well width to be controlled down to one monolayer. However, the etching results in QWIS with thicknesses varying within several percent along the structure. The fractional-layer superlattice technology used for fabrication of QWIS [12, 13] allows one to obtain structures with periods as short as 16 nm. However, even improved technologies [14–16] do not provide abrupt interfaces between the GaAs and AlAs layers; as a result L_y and L_z vary with x. Thus, it appears that no current and foreseeable future technologies of fabricating QWIS can ensure the possibility of creating ideal structures with constant thickness. The variation of QWI thickness results in the variation of subband energies. Consequently, electron scattering is no longer energetically coherent in different parts of a QWI [17, 18]; this should lead to the broadening or even complete washing-out of the resonant peaks [19]. This effect has not yet been studied extensively.

The aim of the present paper is to investigate both the phonon confinement and multi-subband structure and to reveal the role of SO phonons and confined longitudinal-optical (LO) phonons in intersubband transitions. Moreover, the resonant scattering peak broadening due to the variation of thickness along the QWI is considered in order to calculate scattering rates in real QWI structures. We will consider a rectangular QWI fabricated of polar semiconductor and embedded in another polar semiconductor. Firstly, all expressions will be given for an ideal QWI (in section 2) and then we will account for variations in QWI thickness (in section 3). In section 4 the numerical results for room temperature will be presented and discussed. The summary and conclusions are given in section 5.

2. Scattering rates in an ideal QWI

The 1D electron wavefunction in a rectangular QWI is of well known form

$$|q_x, j, l\rangle = \frac{1}{\sqrt{L_x}} e^{iq_x x} \left(\frac{2}{L_y}\right)^{1/2} \sin\left(\frac{j\pi y}{L_y}\right) \left(\frac{2}{L_z}\right)^{1/2} \sin\left(\frac{l\pi z}{L_z}\right)$$
$$j = 1, 2, \ldots, l = 1, 2, \ldots. \tag{1}$$

The corresponding energy is

$$E(q_x, j, l) = E_x(q_x) + E_{jl} \tag{2}$$

where

$$E_x(q_x) = \frac{\hbar^2 q_x^2}{2m^*} \tag{3}$$

is the electron kinetic energy, q_x is the electron wavenumber in the x direction, and

$$E_{jl} = \frac{\hbar^2}{2m^*}\left[\left(\frac{j\pi}{L_y}\right)^2 + \left(\frac{l\pi}{L_z}\right)^2\right] \tag{4}$$

is the subband $\{j, l\}$ energy with respect to the bulk ground level. Here L_y and L_z represent QWI dimensions in the y and z directions, respectively. Equation (1) represents the wavefunction for a carrier in a waveguide supporting standing modes in the y and z directions and travelling in the x direction of the QWI. The interaction Hamiltonians for SO and confined LO modes are as given in [4]. The form of LO phonon Hamiltonian reflects the fact that confined LO phonons in a QWI have a mode structure similar to the electromagnetic modes in a dielectric waveguide. For the evaluation of electron scattering rates in an ideal QWI, we assume the Fermi golden rule to be valid. (The validity of this approach is discussed in detail in [2–7, 20–22].) Note that we are dealing with high temperatures where quantum interference effects are not important. The transition probability from an initial electron state $|q_x, j, l\rangle$ to a final one $|q_x', j', l'\rangle$ is then as follows

$$W^{\{e/a\}}(q_x, j, l; q_x' j', l') = \frac{2\pi}{\hbar}|M^{\{e/a\}}|^2 \delta\left[E(q_x', j', l') - E(q_x, j, l) \pm \hbar\omega\right] \tag{5}$$

where the superscript 'e' and the upper sign indicates emission, 'a' and the lower sign indicates absorption, and $M^{\{e/a\}}$ is the matrix element for electron–phonon interaction

$$M^{\{e/a\}} = \langle q_x', j', l'; N + 1/2 \mp 1/2 | H^{1D} | q_x j, l; N + 1/2 \pm 1/2\rangle. \tag{6}$$

Summing (5) over all final states and considering the electron wavefunction given by (1) and the interaction Hamiltonian given in [2, 4], then the total electron scattering rate $\overline{\lambda}_{LO}^{\{e/a\}}(q_x, j, l)$ by confined LO phonons from the state $|q_x, j, l\rangle$ to elsewhere can be expressed in a form similar to that of [4]

$$\overline{\lambda}_{LO}^{\{e/a\}}(q_x, j, l) = \sum_{j', l'} \lambda_{LO}^{\{e/a\}}(q_x, j, l; j', l') \tag{7}$$

where the rate of particular intrasubband or intersubband j, l-to-j', l' transitions

$$\lambda_{LO}^{\{e/a\}}(q_x, j, l; j', l') = \frac{e^2}{8\pi^2\epsilon_0}\int_{-\infty}^{+\infty} dk_x \omega_{LO}(N + 1/2 \pm 1/2) I_{LO}(k_x, L_y, L_z) \times \delta\left[E(q_x', j', l') - E(q_x, j, l) \pm \hbar\omega_{LO}\right] \delta_{q_x', q_x \mp k_x} \tag{8}$$

is found by integrating (5) over phonon wavenumber k_x within one particular final subband j', l'. Here,

$$I_{LO}(k_x, L_y, L_z) = \left(\frac{1}{\kappa_\infty} - \frac{1}{\kappa_0}\right)\frac{(2\pi)^2}{L_y L_z} \times \sum_{m=1,2,3,\ldots}\sum_{n=1,2,3,\ldots}\left\{\frac{4P_{mn}}{[k_x^2 + (m\pi/L_y)^2 + (n\pi/L_z)^2]^{1/2}}\right\}^2 \tag{9}$$

with

$$P_{mn} = \int_0^{L_y} \mathrm{d}y \frac{2}{L_y} \int_0^{L_z} \mathrm{d}z \frac{2}{L_z} \sin\left(\frac{j\pi y}{L_y}\right) \sin\left(\frac{j'\pi y}{L_y}\right) \sin\left(\frac{l\pi z}{L_z}\right) \times \sin\left(\frac{l'\pi z}{L_z}\right) \sin\left(\frac{m\pi y}{L_y}\right) \sin\left(\frac{n\pi z}{L_z}\right). \tag{10}$$

It has been shown [4] that in the EQL the dominant contribution to the sum over phonon modes is made by the first mode with $m = n = 1$ and the simple approximation for the scattering rate has been derived. In multi-subband structures the higher modes might influence the scattering rates considerably, so generally we have to take the sum over all modes. The number of subbands considered, however, limits the number of 'active' modes which contribute significantly to the scattering rates. For instance, from the analogy with the EQL case, the intrasubband scattering ($j' = j, l' = l$) in the upper subbands is dominated primarily by the LO phonon modes with $m = j$, $n = l$. That is why the scattering rate decreases with an increase of subband indexes j and l due to an increase of the denominator in (9).

The electron transition rate due to SO phonons can be given by [3, 4]

$$\lambda_{\mathrm{SO}}^{\{\mathrm{e/a}\}}(q_x, j, l; j', l') = \frac{e^2}{8\pi^2\epsilon_0} \int_{-\infty}^{\infty} \mathrm{d}k_x \omega_{\mathrm{SO}}(N + 1/2 \pm 1/2) I_{\mathrm{SO}}(k_x, L_y, L_z) \times \delta[E(q_x', j', l') - E(q_x, j, l) \pm \hbar\omega_{\mathrm{SO}}]\, \delta_{q_x', q_x \mp k_x} \tag{11}$$

where

$$I_{\mathrm{SO}}(k_x, L_y, L_z) = (2\pi C' P_{\mathrm{SO}}/\omega_{\mathrm{SO}})^2 \tag{12}$$

where C' is the normalization constant,

$$P_{\mathrm{SO}}^{\mathrm{s}} = \frac{1}{\cosh(\alpha L_y/2)\cos\mathrm{h}(\beta L_z/2)} \int_0^{L_y} \mathrm{d}y \frac{2}{L_y} \int_0^{L_z} \mathrm{d}z \frac{2}{L_z} \times \sin\left(\frac{j\pi y}{L_y}\right) \sin\left(\frac{j'\pi y}{L_y}\right) \sin\left(\frac{l\pi z}{L_z}\right) \sin\left(\frac{l'\pi z}{L_z}\right) \times \cosh\left[\alpha\left(y - \frac{L_y}{2}\right)\right] \cosh\left[\beta\left(z - \frac{L_z}{2}\right)\right] \tag{13}$$

for symmetric modes, and

$$P_{\mathrm{SO}}^{\mathrm{a}} = \frac{1}{\sinh(\alpha L_y/2)\sinh(\beta L_z/2)} \int_0^{L_y} \mathrm{d}y \frac{2}{L_y} \int_0^{L_z} \mathrm{d}z \frac{2}{L_z} \times \sin\left(\frac{j\pi y}{L_y}\right) \sin\left(\frac{j'\pi y}{L_y}\right) \sin\left(\frac{l\pi z}{L_z}\right) \sin\left(\frac{l'\pi z}{L_z}\right) \times \sinh\left[\alpha\left(y - \frac{L_y}{2}\right)\right] \sinh\left[\beta\left(z - \frac{L_z}{2}\right)\right] \tag{14}$$

for antisymmetric modes. Parameters α and β are defined by the following relations

$$\alpha^2 + \beta^2 - k_x^2 = 0 \tag{15}$$

and

$$\alpha L_y = \beta L_z. \tag{16}$$

The SO phonon frequency ω satisfies the dispersion relation

$$\kappa_1(\omega)\tanh(\alpha L_y/2) + \kappa_2(\omega) = 0 \qquad \text{(symmetric modes)} \tag{17}$$

$$\kappa_1(\omega)\coth(\alpha L_y/2) + \kappa_2(\omega) = 0 \qquad \text{(antisymmetric modes)} \tag{18}$$

Here κ_1 and κ_2 are dielectric functions of the QWI material and the surrounding material, respectively. In the case of the EQL, the integration of (14) yields zero, i.e. electron–SO-phonon intrasubband scattering is due to symmetric modes alone. Electron intersubband transitions are, however, due to scattering by both symmetric and antisymmetric SO modes. The selection rules for these transitions follow directly from (13) and (14). From symmetry it is evident that intersubband transitions due to symmetric modes are allowed when both subband indexes change by even numbers, while transitions due to antisymmetric modes are allowed when both indexes change by odd numbers. The intersubband transitions due to SO phonons where one index changes by an even number and another index by an odd number are forbidden by selection rules for both symmetric and antisymmetric SO modes. Due to the identical formulation of (8) and (11) the general expression for the total electron scattering rate from the state $|q_x, j, l\rangle$ to elsewhere due to either LO or SO phonons can be written by taking into consideration equation (7) and the similar equation for SO phonons. Noting that only forward and backward electron scatterings are possible, the integral over phonon wavenumber can be changed by the sum over two possible phonon wavenumbers

$$\overline{\lambda}^{\{e/a\}}(q_x, j, l) = \frac{e^2}{8\pi^2\epsilon_0\hbar}\left(\frac{m^*}{2}\right)^{1/2} \times \sum_{j',l'} \sum_{k_x = k_+^{\{e/a\}}, k_-^{\{e/a\}}} \omega(N + 1/2 \pm 1/2) I(k_x, L_y, L_z) \frac{1}{\sqrt{E_x'}} \tag{19}$$

where $E_x' = E_x + E_{jl} - E_{j'l'} \pm \hbar\omega$ is the electron kinetic energy after scattering, and phonon wavenumbers k_x are

$$k_\pm^{\{e\}} = q_x \pm \sqrt{2m^* E_x'}/\hbar \tag{20}$$

$$k_\pm^{\{a\}} = -q_x \pm \sqrt{2m^* E_x'}/\hbar. \tag{21}$$

Note that the plus and minus signs in (20) and (21) correspond to forward and backward electron scattering, respectively, for absorption, and to backward and forward scattering, respectively, for emission, if the electron initial wavenumber is positive, and vice versa if the initial wavenumber is negative. The divergence in (19) resides in the square root of the final electron energy in the denominator, which represents the density of final states in the ID system. The rest of (19) depends smoothly on electron energy through the phonon wavenumber k_x.

3. Scattering rates in a real QWI

In the previous section we have considered an ideal QWI with a constant cross section along the structure. A unique feature of ideal 1D electron systems is the divergent nature of the density of states at zero kinetic energy appearing through the square root in the denominator of (19). That is why the multiple sharp (diverging) peaks on the energy dependences of the scattering rates are observed. Real QWIs always have a variable thickness, as we have already discussed in the introduction. Now, let us consider a real QWI with variable thickness. It is evident from (2)–(4) that the variation of a structure thickness causes the variation in subband energy, $E_{jl}(x)$. Since the total electron energy does not depend on the QWI thickness, the variation of E_{jl} with x results in the variation of electron kinetic energy E_x. For the sake of simplicity in the analytical considerations, we assume $L_y = L_z = d(x)$ in this section, where $d(x) = d_0 + \delta d(x)$ with the condition $\delta d(x) \ll d_0$ for all x. Note that our model implies that the variation is a smooth function of x and the characteristic length of the fluctuations is much greater than the de Broglie wavelength. Since the total electron scattering rate given by (19) is expressed by the sum over all possible final states, we can analyse one separate term of the sum in (19) representing the rate of some particular electron transition regardless of the phonon mode (SO or LO) assisting that transition. For the sake of convenience we will use the same notation λ for this particular transition rate, but now as a function of electron kinetic energy. (Indeed each term in (19) depends on the QWI thickness through the function I (9), (12), and the dependence on E_x appears through E'_x and the phonon wavenumber k_x.) The transition rate averaged over the QWI length is given by

$$\lambda(E_0, d_0) = \frac{1}{L}\int_0^L \mathrm{d}x\, \lambda[E_x(x), d(x)] \tag{22}$$

where $E_x = E_0 + \delta E(x)$, $E_0 = E - \langle E_{jl}\rangle$ is the electron kinetic energy corresponding to a given total energy E and average subband position $\langle E_{jl}\rangle$, and $\delta E(x)$ is the electron kinetic energy variation (opposite to the variation of subband position) due to the variation of QWI thickness. The total electron energy given by (2) remains constant while the increment in the electron kinetic energy due to an increment in the thickness δd can be expressed in the linear approximation $\delta d(x) \ll d_0$ as

$$\delta E = (\hbar^2/2m^*)\left[(j\pi/d_0)^2 + (l\pi/d_0)^2\right] 2\delta d/d_0 \equiv \langle E_{jl}\rangle 2\delta d/d_0 \tag{23}$$

or

$$\delta E/\langle E_{jl}\rangle = 2\delta d/d_0. \tag{24}$$

In other words, the increment in the electron kinetic energy is proportional to the increment in the thickness, and the proportionality constant depends on the subband indexes. It is seen from (23) that for the same fluctuation in thickness the fluctuation in electron kinetic energy is larger in higher subbands. Note that the averaging over the structure length in (22) yields significant changes in the electron scattering rate only in the regions where $\lambda(E_x, d)$ is strongly dependent on E_x (i.e. close to the divergence points). The changes due to the direct dependence of the scattering rate on structure thickness d are relatively small because ω and I in (19) are both smooth

functions of d and the limits of variation of d are narrow ($\delta d \ll d_0$). Consequently, the averaging over structure length can be approximated, with sufficient accuracy, by the averaging over electron kinetic energy alone:

$$\lambda(E_0, d_0) = \int_{E_0-\Delta E}^{E_0+\Delta E} \mathrm{d}E_x \, \lambda(E_x, d_0) F(E_x) \tag{25}$$

where $\Delta E = \max|\delta E(x)|$, and $F(E_x)$ is the probability density for an electron of having kinetic energy E_x from the interval $(E_0 - \Delta E, E_0 + \Delta E)$ at a given total electron energy E,

$$\int_{E_0-\Delta E}^{E_0+\Delta E} \mathrm{d}E_x \, F(E_x) = 1. \tag{26}$$

The physical requirement for the integration limits is $\Delta E < E$, which is also implied by the condition $\delta d \ll d_0$. It is convenient to express the scattering rate for each possible transition by separating the diverging part from the rest of (19):

$$\lambda(E_x, d_0) = P(E_x, d_0)\Theta(E'_x)(E'_x)^{-1/2} \tag{27}$$

where $P(E_x, d_0)$ represents the non-diverging part of (19), Θ is the step function which cuts off the scattering rate below zero electron final energy E'_x. For the purpose of making qualitative estimations, we consider the simplest case of a uniform energy distribution, i.e. completely random fluctuations of QWI thickness. Then by assuming that the smooth function $P(E_x, d)$ depends weakly on E_x within the narrow interval of energy variation and that the scattering rate given by (27) is a function of electron final energy alone, we can easily integrate (22) over the final energy variation and obtain:

$$\lambda(E_0, d_0) = (P(E_0, d_0)/\Delta E')[\Theta(E'_0 + \Delta E')(E'_0 + \Delta E')^{1/2} - \Theta(E'_0 - \Delta E')(E'_0 - \Delta E')^{1/2}]. \tag{28}$$

If we put $E'_0 = 0$ in (28) we get:

$$\lambda(E_i, d_0) = P(E_i, d_0)/\sqrt{\Delta E'} \tag{29}$$

i.e. the scattering rate is no longer divergent. $E'_0 = E' - \langle E_{j'l'} \rangle$ is the average final electron kinetic energy corresponding to the final total electron energy $E' = E \pm \hbar\omega$; $\Delta E' = \max|\delta E'(x)|$ is the amplitude of electron final energy variation in the final subband j', l'; and E_i is the threshold initial electron kinetic energy corresponding to the zero final electron energy.

The form of (27) suggests a compact and convenient way of storing the scattering rates in a Monte Carlo program. If we tabulate the scattering rates, then we must use a rather small or variable energy step in order to keep all the peculiarities of the sharp peaks. For multi-subband structures this method requires a lot of computer memory and calculation of the scattering rates for each scattering event is time consuming. However, we can store the tabulated $P(E_x, d)$ part of (27) alone and combine it with the calculated square root. This method should require a little more execution time but, noting that $P(E_x, d)$ is a smooth function of E_x, one can use a much larger energy step and save a lot of computer memory.

4. Results and discussion

We present here the results of numerical calculations performed for a GaAs QWI of dimensions $L_y = 150$ Å and $L_z = 250$ Å embedded in AlAs. We have considered 11 subbands. The summation in (9) has been performed over phonon modes from $m, n = 1$ to $m, n = 11$. The calculated energy dependence of the total electron–LO-phonon scattering rate from the first subband to elsewhere, including itself (i.e. both intrasubband and intersubband transitions), is presented in figure 1 for the case of an ideal QWI. Figure 2 shows the same dependence for electron–SO-phonon scattering. Forward and backward scattering are plotted as separate scattering mechanisms in order to reveal the polar character of electron interaction with LO and SO modes. Indeed, electron forward scattering is dominant both for LO and SO phonons. The multiple sharp peaks on the 'backward' curves of figure 2 are almost unnoticeable on the 'forward' curves. This is because, in the 'forward' curve due to the SO modes, the relatively low intersubband scattering rates (from the first subband) are plotted against the background of strong intrasubband scattering. For backward scattering, the strength of intrasubband scattering is reduced by more than three orders of magnitude. As a result, intersubband transition peaks are well pronounced. Note that peaks on figures 1 and 2 are finite due to finite energy steps of integration. The maxima tend to infinity as the energy step tends to zero, as is evident from (19) (note that forward and backward scattering rates are equal at energies infinitely close to the point of divergence). This is why, for the sake of mathematical accuracy, we should also mark infinitely high and narrow peaks on 'forward' curves of figure 2. However, these peaks are not realistic physically for real QWI structures. Comparing figures 1 and 2, one can see that some peaks seen in figure 1 disappear in figure 2 as a result of forbidden transitions due to SO phonons related to those peaks (see the discussion in section 2). On the other hand, all peaks related to allowed intersubband transitions are doubled in figure 2. This is due to the fact that SO phonon modes in GaAs/AlAs QWI split into two branches; one is related to GaAs and the other to AlAs. Their frequencies are considerably different; the GaAs-like mode is shifted towards lower frequencies than those of LO phonons [4].

To reveal the pecularities of electron intersubband scattering by SO phonons, we have plotted the rates of particular intersubband transitions in figures 3 and 4. The obvious tendency is a decrease in the rate of intersubband transitions as the intersubband energy separation (i.e. $|E_{jl} - E_{j'l'}|$) increases. This tendency, however, does not always occur. When the intersubband energy separation is close to the SO phonon (GaAs- or AlAs-like) energy, the phonon wavenumber k_z is close to zero. This is the so-called resonant intersubband electron–SO-phonon scattering condition [7]. The electron–SO-phonon scattering rate is inversely proportional to the fourth power of the phonon wavenumber k_z (this proportionality appears through the parameters α and β when integrating (13) [4]) and tends to infinity for any electron energy when the intersubband energy separation approaches the SO phonon energy! Either an increase or a decrease in the intersubband energy separation causes a reduction in the scattering rate. In our particular structure, the energy separations between the 2nd and 3rd, the 5th and 7th, and the 10th and 11th subbands are close to the AlAs-like SO phonon energy. Therefore, we should observe resonant electron–SO-phonon scattering between these subbands. However, transitions between these subbands are forbidden by selection rules. Nevertheless, it is possible to create QWIs with subbands in resonance where resonant intersubband transitions are allowed. In order to verify

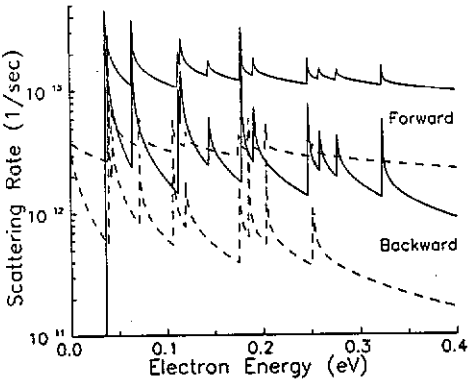

Figure 1. Electron–LO-phonon scattering rates in/from the 1st subband (i.e. both intrasubband and intersubband transitions) as a function of electron kinetic energy. Solid curves, emission; dashed curves, absorption. Upper curves, forward electron scattering (wavevector direction does not change), lower curves, backward scattering (wavevector direction reverses). Scattering from the 1st subband to all eleven subbands (including scattering into the 1st subband itself) is considered. The lattice temperature is assumed to be 300 K; the QWI dimensions are $L_y = 150$ Å and $L_z = 250$ Å.

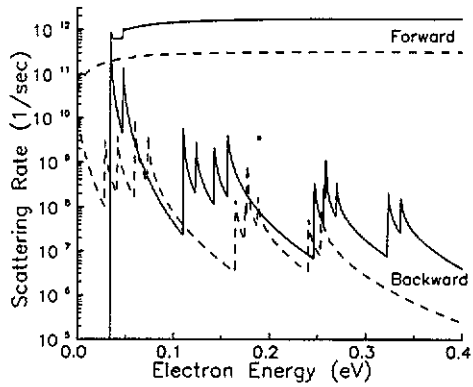

Figure 2. Electron–SO-phonon scattering rates in/from the 1st subband as a function of electron kinetic energy. The notation is the same as in figure 1.

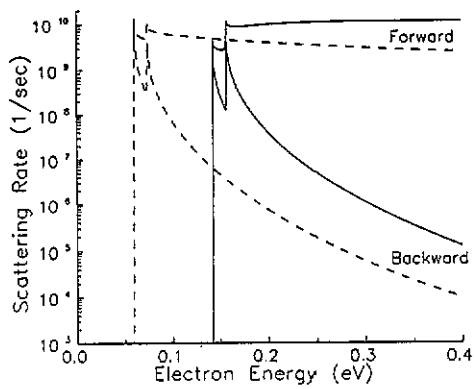

Figure 3. Electron transition rates from the 1st to the 5th subband due to SO phonons as a function of electron kinetic energy. The notation is the same as in figure 1.

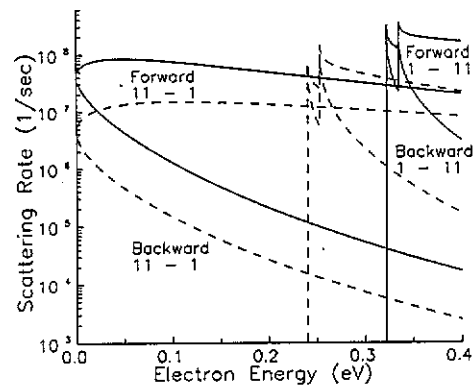

Figure 4. Electron transition rates from the 1st to the 11th subband and from the 11th to the 1st subband due to SO phonons as a function of electron energy with respect to the bottom of the 1st subband. The notation is the same as in figure 1.

this statement we have also considered a model structure with allowed transitions between subbands in resonance. The transition rates between these subbands exceed all other scattering rates by SO phonons and are comparable to, or even higher than, electron–LO-phonon scattering rates (numerical results are not presented here). Note that here we deal with the resonance with respect to the intersubband energy

separation, but not with respect to the electron energy. Electron–confined-LO-phonon scattering is not influenced significantly by the resonant intersubband scattering condition because, in the denominator of (9), there is the total phonon wavenumber with non-vanishing transverse components at finite L_y and L_z. However, in the 3D limit when L_y and L_z tend to infinity, the transverse components tend to zero and the electron–LO-phonon scattering becomes sensitive to the resonant conditions. That is why Briggs *et al* [7] have observed resonant intersubband electron scattering by 3D LO phonons. The intrasubband electron scattering rate due to SO phonons depends weakly on subband number, whereas the intrasubband scattering rate due to confined LO phonons decreases slightly due to the increase of the number of 'active' phonon modes and the denominator in (9). This fact has been anticipated when analysing scattering rates. Thus, the results presented clearly demonstrate that intrasubband electron scattering in such structures is dominated primarily by confined LO modes, but in some particular (resonant) intersubband transitions the same or even the dominant role may be played by SO phonons.

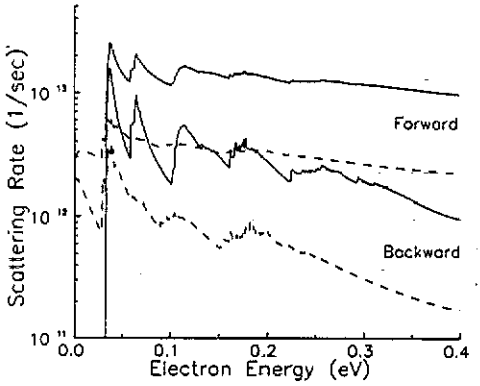

Figure 5. Electron–LO-phonon scattering rates in/from the 1st subband when the surface roughness is included. The effect of surface roughness is considered by averaging the scattering rates over the length of the QWI with variable thickness given by $L_y = L_{y0} + \delta L_y \cos(Kx)$ and $L_z = L_{z0} + \delta L_z \cos(2Kx)$ with $\delta L_y/L_{y0} = \delta L_z/L_{z0} = 0.05$. The notation is the same as in figure 1.

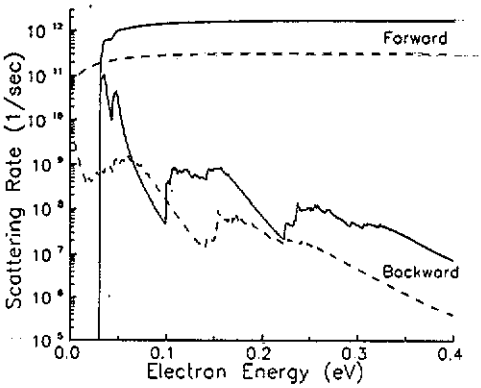

Figure 6. Electron–SO-phonon scattering rates in/from the 1st subband when the surface roughness is included. The effect of surface roughness is considered, as described in figure 5. The notation is the same as in figure 1.

The calculations of the scattering rates in real QWIs have been performed with the same model of scattering processes as in ideal QWIs, but with variable thicknesses L_y and L_z. We have assumed that the thickness varies with the harmonic law. The amplitudes of variation, δL_y and δL_z, have been chosen to be a fraction 0.01 to 0.1 of the corresponding thicknesses L_y and L_z. It is evident that the results of averaging do not depend on the period of the variation, but they might depend on the mutual phases of the variation of L_y and L_z. Therefore we have considered three cases: $L_z = L_{z0} + \delta L_z \cos(Kx)$, $L_z = L_{z0} + \delta L_z \sin(Kx)$, and $L_z = L_{z0} + \delta L_z \cos(2Kx)$, with $L_y = L_{y0} + \delta L_y \cos(Kx)$ in all cases. It has been found that the results do not show a significant difference between these models. Figures 5 and 6 demonstrate the typical results obtained for a reasonable 5% variation

amplitude ($\delta L_y/L_{y0} = \delta L_z/L_{z0} = 0.05$). Compared to figures 1 and 2 (calculated for the corresponding ideal QWI), one can see that such variations in thickness yield considerable broadening and reduction of the very first scattering peaks and the complete disappearance of the peaks at higher energies. Similar curves with a different degree of broadening are obtained for other variation amplitudes. Even a variation amplitude as small as 1% leads to the disappearance of the divergence at the resonant energies and essential smearing out of the peak-like structure on the curves discussed. Similar results are provided by the simplified model of equation (28).

5. Conclusion

In this paper, we have demonstrated that intrasubband electron scattering in GaAs/AlAs QWIs is dominated primarily by confined LO phonons, while electron intersubband transitions under certain conditions are strongly affected by SO phonons. A unique feature of the electron–SO-phonon scattering in QWIs is its resonant dependence on the intersubband energy separation. When the intersubband energy separation approaches the SO phonon energy, the electron–SO-phonon scattering rate tends to infinity at any electron energy. The scattering rates in the QWIs with variable thickness exhibit no divergence at the resonant energies as a result of the variation of subband energies. The peak-like structure smears out even for a very small wire thickness fluctuation. The peak-like dependence disappears for 5% fluctuations of QWI thickness. It is very important to stress here that the influence of the QWI cross section fluctuation on the scattering rate seems at first glance to be similar to the influence of impurity scattering [23]. In spite of this similarity, the effects of broadening on electron transport in QWIs are completely different [19]. The broadening due to scattering [23] is homogeneous along a QWI, and in fact introduces new channels for the current so that the calculated conductivity is an average conductivity of these parallel channels. The channels with the largest conductivity give the major contribution to the average conductivity. That is why such broadening practically does not change the resistivity if only one quantum level is filled. In our case the conductivity fluctuates along the QWI; the system is analogous to the series connections of resistors and the major contribution to the resistivity comes from the high-resistance parts of the QWI. Hence the narrowest part of the QWI defines its conductivity. More rigorous results on transport phenomena in real QWIs will be discussed elsewhere.

Acknowledgments

The authors would like to thank Professor M A Littlejohn and Dr J Mink for helpful discussions. The work performed at North Carolina State University is supported, in part, by the Office of Naval Research under grant No N00014-90-J-1835 and by the US Army Research Office under grant No DAAL03-89-D-0003-05.

References

[1] Sakaki H 1980 *Japan. J. Appl. Phys.* **19** L735
[2] Stroscio M A 1989 *Phys. Rev.* B **40** 6428
[3] Stroscio M A, Kim K W, Littlejohn M A and Chuang H 1990 *Phys. Rev.* B **42** 1488

[4] Kim K W, Stroscio M A, Bhatt A, Mickevičius R and Mitin V V 1991 *J. Appl. Phys.* **70** 319
[5] Briggs S and Leburton J P 1988 *Phys. Rev.* B **38** 8163
[6] Briggs S and Leburton J P 1989 *Superlatt. Microstruct.* **5** 145
[7] Briggs S, Jovanovic D and Leburton J P 1989 *Appl. Phys. Lett.* **54** 2012
[8] Watt M, Sotomayor-Torres C M, Amot H E G and Beaumont S P 1990 *Semicond. Sci. Technol.* **5** 285
[9] Fasol G, Tanaka M, Sakaki H and Horikosh Y 1988 *Phys. Rev.* B **38** 6056
[10] Forchel A, Maile B E, Leier H, Mayer G and Germann R 1990 *Phys. Status Solidi* b **159** 457
[11] Smith H I, Ismail K, Chu W, Yen A, Ku Y C, Schattenberg M L and Antoniadis D A 1989 *Nanostructure Physics and Fabrication* ed M A Reed and P Kirk (Boston: Academic) p 57
[12] Petroff M P, Gossard A C and Wiegman W 1984 *Appl. Phys. Lett.* **45** 620
[13] Fukui T, Saito H, Tokura Y, Tsubaki K and Susa N 1990 *Surf. Sci.* **228** 20
[14] Petroff P M, Tsuchiya M and Coldren L A 1990 *Surf. Sci.* **228** 24
[15] Gaines J M, Petroff P M, Kroemer H, Simes R J, Geels R S and English J H 1988 *J. Vac. Sci. Technol.* B **6** 1378
[16] Colas E, Symhony S, Kapon E, Bhat R, Hwang D M, Lin P S D 1990 *Appl. Phys. Lett.* **57** 914
[17] Warren A C, Antoniadis D A and Smith H I 1986 *Phys. Rev. Lett.* **56** 1858
[18] Bagwell P F, Antoniadis D A and Orlando T P 1989 *VLSI Electronics Microstructure Science: Advanced MOS Device Physics* vol 18, ed N G Einspruch and G Gildenblat (New York: Academic) pp 305–55
[19] Mitin V V 1990 *Superlatt. Microstruct.* **8** 413
[20] Hu G Y and O'Connell R F 1990 *Phys. Rev.* B **42** 1290; 1990 *J. Phys.: Condens. Matter* **2** 9381
[21] Bagwell P F 1990 *Phys. Rev.* B **41** 10354
[22] Kumar A and Bagwell P F 1991 *Phys. Rev.* B **43** 9012
[23] Das Sarma S and Xie X C 1987 *Phys. Rev.* B **35** 9875